ISTITUTO NAZIONALE DI FISICA NUCLEARE - ISTITUTO NAZIONALE DI FISICA NUCLEARE - ISTITUTO NAZIONALE DI FISICA NUCLEARE - ISTITUTO NAZIONALE DI FISICA NUCLEARE - ISTITUTO NAZIONALE DI FISICA NUCLEARE - ISTITUTO NAZIONALE DI FISICA NUCLEARE - ISTITUTO NAZIONALE DI

# Laboratori Nazionali di Frascati

LNF-93/041 (P)
29 Luglio 1993

N. Fabiano, A. Grau, G. Pancheri:

## TOPONIUM BOUND STATES AT LHC/SSC

PACS.: 14.80.–j ; 12.40.Qq

Invited Talk at the
*VIII Corso Invernale di Fisica Adronica*
Folgaria, 31 January – 2th February 1993

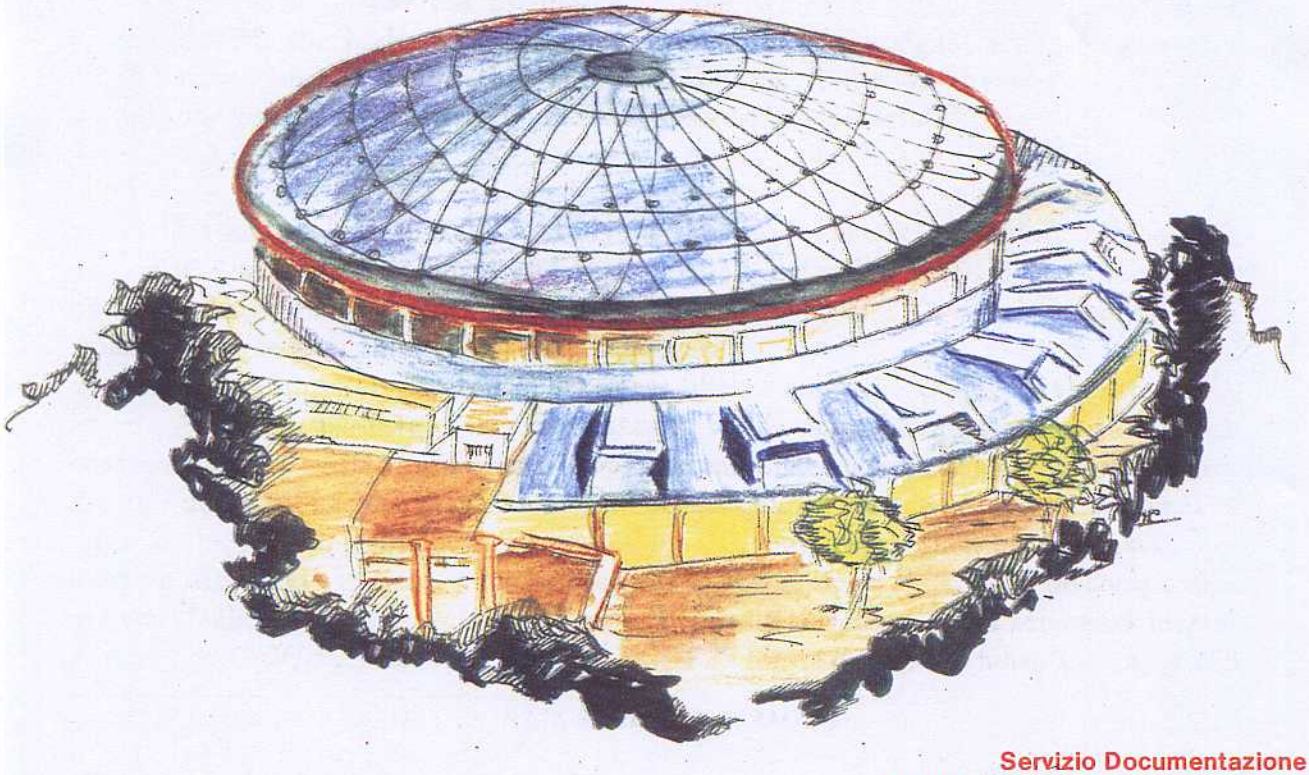

Servizio Documentazione
dei Laboratori Nazionali di Frascati
P.O. Box, 13 - 00044 Frascati (Italy)

INFN - Laboratori Nazionali di Frascati
Servizio Documentazione

LNF-93/041 (P)
29 Luglio 1993

# TOPONIUM BOUND STATES AT LHC/SSC[1]

N.Fabiano
*INFN-Laboratori Nazionali di Frascati, P.O.Box 13, I00044 Frascati ,Italy*
A.Grau
*Physics Department, University of Granada, Granada, Spain*
and
G.Pancheri
*INFN-Laboratori Nazionali di Frascati, P.O.Box 13, I00044 Frascati ,Italy*

*Invited Talk at the VIII Corso Invernale di Fisica Adronica*
Folgaria, 31 January-6th February 1993

## Abstract

We discuss existency conditions for toponium bound states and evaluate the wave function at the origin, comparing different models for the static interquark potential. We evaluate the production cross-section for $J^{PC} = 0^{-+}, 1^{--}$ for the case of a static Coulomb Potential. For the pseudoscalar case, which at LHC and SSC would be produced with the highest cross-section, we compare the signal with the expected QCD background. We find that the present lower limits on the top mass almost exclude the possibility of these bound states and their detectability.

In this lecture, we present a study of the production of toponium states with $J^{PC} = 0^{-+}$ at hadron colliders and their possible detection through the two photon decay mode. We also discuss very briefly the case $J^{PC} = 1^{--}$, which however has a smaller cross-section than the pseudoscalar case.

The lower limits on the top quark mass obtained by the CDF Collaboration [1] , i.e. $m_t \geq m_W + m_b$, have drastically changed the familiar bound state picture which charmonium and bottomium spectroscopy had established, since the top quark can now directly decay into a real $W$-boson and a bottom quark and this decay probability is as large as the one typical of strong interactions. Toponium can then be too unstable to exist for any length of time, since its life-time is becoming so short as to be comparable or even smaller than the revolution time[2]. Typically this happens for top quark masses around 130 $GeV/c^2$. The latest D0 [3] and CDF [4] limits on the top mass, i.e. $m_t \geq 103$

[1]FABIANO@IRMLNF, 16487::IGRAU, PANCHERI@IRMLNF

and 108 $GeV/c^2$ respectively, indicate that there remain a very narrow mass window in which toponium can exist at all, i.e. $216 \leq m_{t\bar{t}} \leq 260\ GeV/c^2$.

In the above energy range, presently planned hadron colliders are good gluon factories and gluon-gluon fusion is the most abundant production mechanism for quark-antiquark bound states. As for the decay channel, at hadron colliders bound states have traditionally been identified through their leptonic or electromagnetic decays, in order to overcome the large hadronic backgrounds. In [5], it has been suggested to search at LHC for the state $J^{PC} = 0^{-+}$ in the two photon decay mode. An estimate of the statistical significance, using realistic LHC type detectors, was done to show that observability of $\eta_t$ was possible for toponium masses in the $200 \div 240\ GeV/c^2$ mass range. The calculation of the signal cross-section is however very sensitive to the estimate of $|\Psi(0)|$, the wave function at the origin. Indeed, the signal cross- section is proportional to the fourth power of the wave function, since $\sigma \approx \frac{\Gamma_i \Gamma_f}{\Gamma_{tot}}$. While both $\Gamma_i$ and $\Gamma_f$ are proportional to $|\Psi(0)|^2$, the total decay width for toponium is dominated by the electroweak single quark decay, which is independent from the value of the wave function at the origin. This is a totally novel situation, quite different from all the other quarkonia states : an uncertainty of as much as 30% on the wave function will produce a difference by more than a factor 4 on the number of observed events. Thus, in [6], the effects of QCD-inspired potential models and that of higher order QCD corrections have been used to obtain a signal cross-section which is a factor 4 to 10 lower than the one in [5]. For this case, the observability of the $\eta_t \rightarrow \gamma\gamma$ signal at LHC is out of question, except for the case $m_{t\bar{t}} \approx 100\ GeV/c^2$ (a possibility now excluded by present experiments [3, 4]) .

In this paper we discuss and compare the different signal cross-sections which are obtained from different potential models. We then compare these estimates with the expected irreducible QCD background, both at LHC as well as at SSC energies . At SSC energies, we notice that, if the high luminosity option [7] $L = 10^{34} cm^{-2} sec^{-1}$ is considered, the signal to noise ratio is acceptable only for toponium masses up to $260\ GeV/c^2$, for the more singular Coulomb-type potential, and up to $\approx 220\ GeV/c^2$ for the so-called QCD potentials.

It then appears that the possibility of observing the process

$$gluon\ gluon \rightarrow \eta_t \rightarrow \gamma\gamma$$

is rather small, although it cannot be excluded yet. We stress, however, the importance of looking for this type of processes: the sensitivity of the cross section to the interquark potential renders it a unique probe of the complete QCD bound state picture .

In Sect.1 we discuss the existency conditions for toponium by comparing different potential model estimates for the $1S - 2S$ splitting with the total toponium decay width. In Sect.2, we present an estimate of the toponium wave function at the origin for a set of potential model predictions and evaluate leptonic and electromagnetic decay widths for the Coulombic case. In Sect. 3 we present the signal cross section for the Coulombic type calculation, for both the pseudo scalar and the vector toponium.

In Sect. 4, the irreducible QCD background is estimated for various kinematic cuts. In Sect. 5 the signal is folded with the experimental resolution and compared to the expected background. The expectations from a QCD-type potential are discussed in the same section, while Sect.6 is dedicated to evaluate the signal to noise ratio at LHC and SSC for an optimized gamma detector, both for the Coulombic as well as for the QCD-type potentials.

# 1 EXISTENCY CONDITIONS

For a top quark with $m_t \geq m_W + m_b$, the total decay rate for a quark-antiquark bound state is dominated by single quark decay into a $W$ boson and a $b$ quark [2, 8]. This decay rate is an increasingly large function of the top quark mass, or in other words, the lifetime of the top quark becomes shorter and shorter as its mass becomes larger. When the decay width overtakes the level splitting between the bound states, no formation of the bound state is envisaged, and the top quark decays before completing a revolution. While the single quark decay width is fully determined from electroweak interactions through the expression

$$\Gamma(t \to Wb) = \frac{G_F m_t^3}{8\pi\sqrt{2}} \left(\frac{2p}{m_t}\right) \left[\left(1 - \frac{m_b^2}{m_t^2}\right)^2 + \frac{m_W^2}{m_t^2}\left(1 + \frac{m_b^2}{m_t^2}\right) - 2\frac{m_W^4}{m_t^4}\right] \qquad (1)$$

with $p$ the $W$-boson momentum in the $t$-quark rest frame, the splitting between the energy levels of the bound states depends upon the strength of the strong force between the quarks and their relative distance[9]. For light quarks one can expect long range confining forces to be dominant, whereas for the top quark the Coulomb part of the potential, i.e.

$$V_Q = -\frac{4}{3}\frac{\alpha_S}{r} \qquad (2)$$

should be the dominant one[10]. Corrections for Higgs boson exchange Yukawa type forces can also be expected[11, 12], but, for a top quark with mass less than $\approx 200\ GeV$, they are small, with an attractive potential for the quark-antiquark singlet state, and may amount to no more than 10% of the Coulomb term. On the other hand, higher order QCD corrections to the potential can be included in $\alpha_s$ through its two loops expression, as shall be discussed in what follows.

To begin with, it is instructive to discuss the top-antitop bound states using a Coulomb potential with QCD couplings and $\alpha_s$ evaluated at a fixed distance $r$, which can be plausibly chosen to be the Bohr radius of the bound state. In this case, the non-relativistic Schroedinger equation can be exactly solved[9] and one can easily evaluate binding energies and the wave function at the origin. The use of a non-relativistic treatment can be justified because the presently rather high limits on the top mass, $m_t \geq 108\ GeV$ [4] imply for the heavy quark velocity $\beta_Q \approx \alpha_s(M_{Q\bar{Q}}^2) \approx 0.1 \div 0.2$. Then

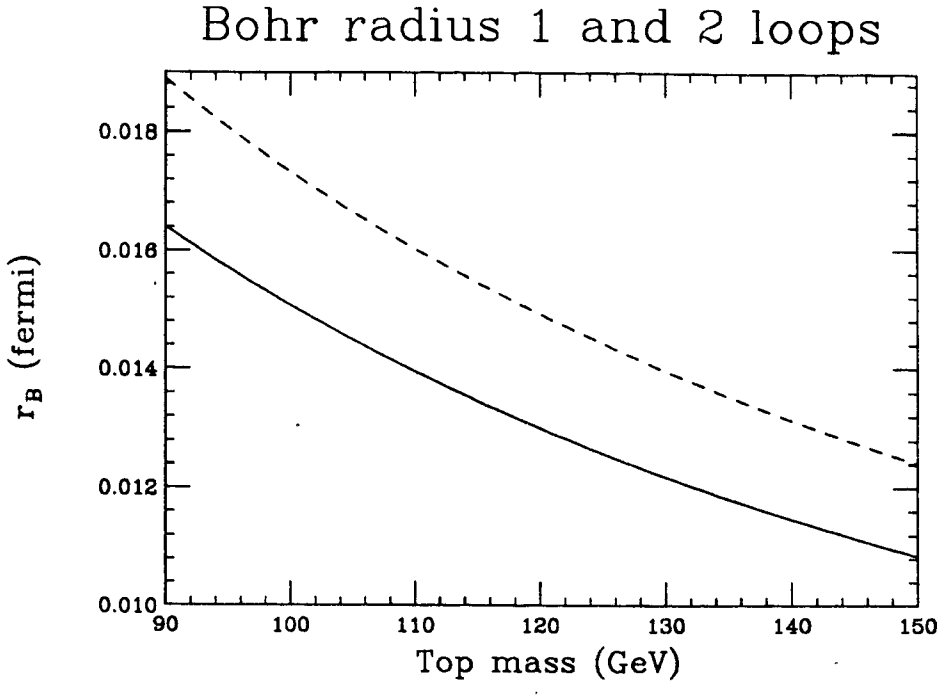


Figure 1: Bohr Radius for Coulombic potential , vs. top mass, for one (full line) and two loop (dashes) $\alpha_s$, with $N_F = 5$, $\Lambda_{\overline{MS}} = 0.2\ GeV$.

the relativistic corrections, which are of order $\beta_Q^2$, can be expected to be $\approx 1 \div 4\%$. Treating the top-antitop system as a non-relativistic hydrogen atom, with a non-running (in $r$) coupling constant for the potential, allows for the use of analytical formulae, from which estimates for decay rates and production cross-sections can be extracted immediately. As we shall see later, the use of the Coulombic potential gives results similar to those with a running (in $r$) $\alpha_s$, for the case in which a two loop $\alpha_s$ is used.

For the Coulombic type potential with a non running $\alpha_s$, the energy levels are given by

$$E_n = -\frac{4}{9n^2} m_t \alpha_s^2 \tag{3}$$

and the Bohr radius of the state is given by

$$r_B = \frac{3}{2\alpha_s m_t} \tag{4}$$

Then, the scale at which to evaluate $\alpha_s$ can be extracted from the above equation with $\alpha_s = \alpha_s(1/r_B)$. In fig.1 we show $r_B$ as a function of the top quark mass and using both the one and the two loops expression for $\alpha_s$, i.e.[10, 13]

$$\alpha_s^{(1)} = \frac{12\pi}{23 log[(1/r_B \Lambda_{\overline{MS}})^2]} \quad and \quad \alpha_s^{(2)}(r) = \frac{4\pi}{b_0 f(r)} \left\{ 1 + \frac{c}{f(r)} - \frac{b_1}{b_0^2} \frac{\log[f(r)]}{f(r)} \right\} \tag{5}$$

with

$$f(r) = \log\left[\frac{1}{(\Lambda_{\overline{MS}} r)^2} + b\right], \quad c = \frac{1}{b_0}\left(\frac{93 - 10N_f}{9}\right) + 2\gamma_E \tag{6}$$

$$b_0 = 11 - \frac{2}{3}N_f, \quad b_1 = 102 - \frac{38}{3}N_f \tag{7}$$

where $\Lambda_{\overline{MS}}$ is the QCD constant and $N_f$ the number of flavours.

With the values for $\alpha_s$ extracted from the figure, one can now calculate the level splitting for the Coulombic potential and compare it both with the splitting from various potential models , as well as with the toponium width.

The potentials we have considered can be grouped in four types:

- 1. Cornell type potential:

$$V(r) = -\frac{k}{r} + \frac{r}{a^2} \tag{8}$$

with

| *Parameters* | *Cornell (A)* | *Cornell (B)* |
|---|---|---|
| $a$ | 2.34 | 2.09 |
| $k$ | 0.52 | 0.3 |

This potential [14] is as singular as the Coulombic one and its strength at the origin is close to the one obtainable from the one loop expression.

- 2. Richardson potential [15]:

$$V_R(r) = -\frac{4}{3}\frac{12\pi}{33 - 2N_f}\int \frac{d^3q}{(2\pi)^3}\frac{e^{iqr}}{q^2\log(1 + q^2/\Lambda^2)} \tag{9}$$

$N_f = 3$ and $N_f = 5$ , $\Lambda = 398\ MeV$

It is possible to write it in the following form:

$$V_R(r) = \frac{8\pi}{33 - 2N_f}\Lambda\left(\Lambda r - \frac{f(\Lambda r)}{\Lambda r}\right) \tag{10}$$

$$f(t) = \left[1 - 4\int_1^\infty \frac{dq}{q}\frac{e^{-qt}}{[\log(q^2 - 1)]^2 + \pi^2}\right] \tag{11}$$

- 3. Potential $V_J$ of Igi-Ono [16, 17]:

$$V_J(r) = V_{AR}(r) + dre^{-gr} + ar \tag{12}$$

$$V_{AR}(r) = -\frac{4}{3}\frac{\alpha_s^{(2)}(r)}{r} \tag{13}$$

with the parameter set [18]:

| *Parameters* | $N_f = 4, \quad b = 20$ | | |
|---|---|---|---|
| $\Lambda_{\overline{MS}}\ (GeV)$ | 0.2 | 0.3 | 0.5 |
| $a\ (GeV^2)$ | 0.1587 | 0.1443 | 0.1391 |
| $d\ (GeV^2)$ | 0.2550 | 0.0495 | 1.476 |
| $g\ (GeV)$ | 0.3436 | 0.3280 | 2.955 |

We have also used the same set of parameters $a$, $d$ and $g$ as above with $N_f = 5$, which could be more appropriate for the large masses under consideration. The value $\Lambda_{\overline{MS}} = 0.366\ GeV$, has also been used, with $a$, $d$ and $g$ parameters as for the $\Lambda_{\overline{MS}} = 0.5\ GeV$ case above.

- 4. Power law, Martin-type Potentials [19, 20, 21],

$$V(r) = -8.064 + 6.8698\ r^{0.1} \tag{14}$$

recently revisited by Rosner et al.[22]:

$$V(r) = \frac{\lambda}{\alpha}(r^{\alpha} - 1) + c \tag{15}$$

| *Parameters* | *Rosner et al. (A)* | *Rosner et al. (B)* |
|---|---|---|
| $\alpha$ | -0.14 | -0.12 |
| $\lambda$ | 0.808 | 0.801 |
| c | -1.305 | -0.772 |

In Figs.2 and 3 we show the toponium width, $\Gamma_{t\bar{t}} = 2\ \Gamma_t$ together with the level splitting for the various potential models, as indicated [23].

For low quark masses, the states are well separated and the splitting is larger than the electroweak decay width. However, since the splitting grows linearly with the top mass, whereas the decay width grows like $m_t^3$, there will be a mass value where the decay width "takes over" the splitting. If we assume as existency condition

$$\Delta E_{1S-2S} \geq \Gamma_{t\bar{t}} \tag{16}$$

we see from fig.2 that formation of the bound state in the Coulombic model is possible for top quark masses less than 150 $GeV$. Other potentials, also including higher order

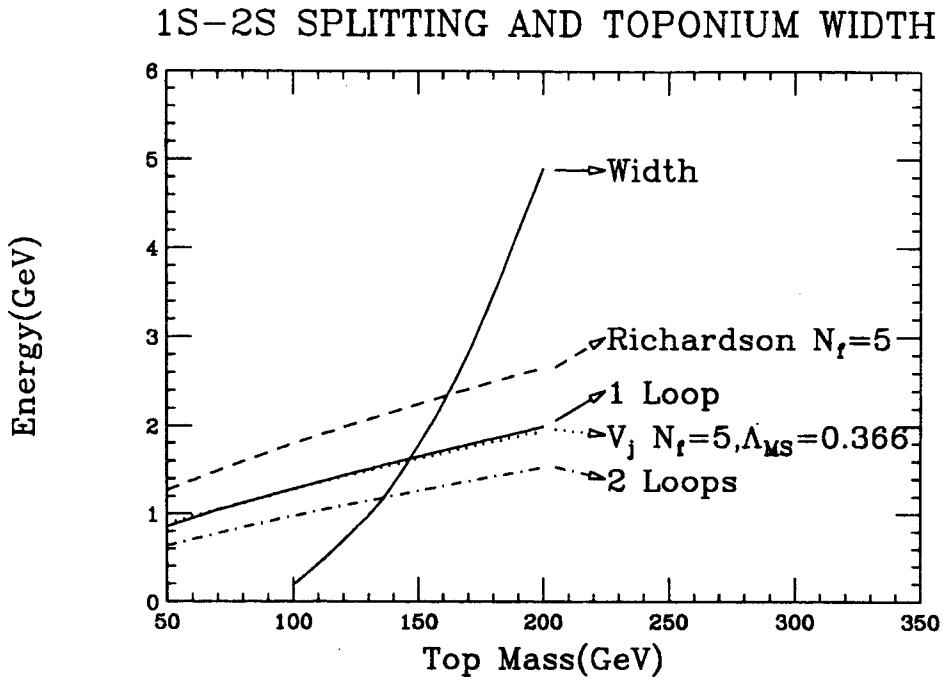


Figure 2: Toponium width (full line) and energy splitting (full and dotdashed lines) for a Coulomb type potential in the Non relativistic Hydrogen like model described in the text, together with other models, vs. top mass.

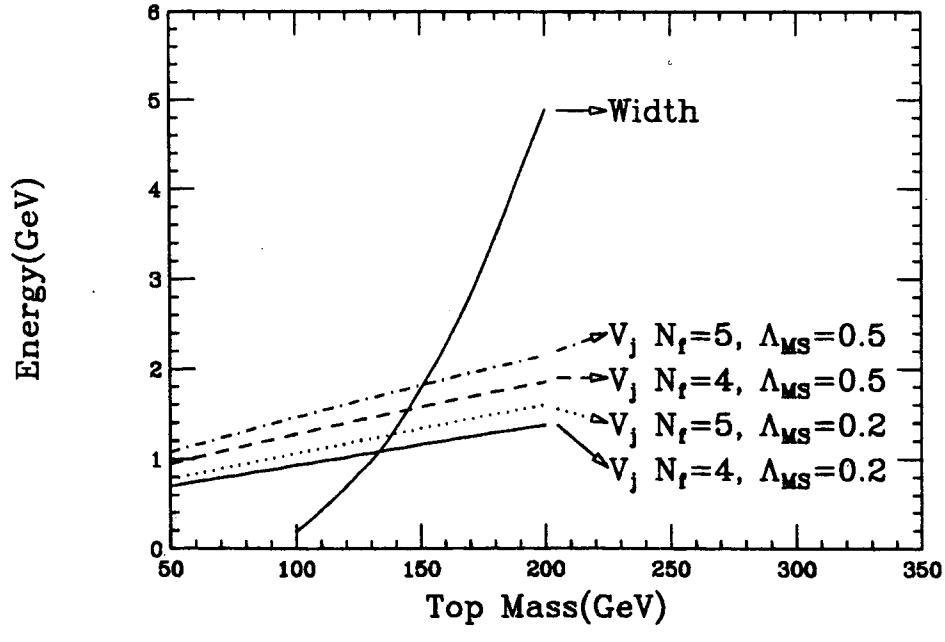


Figure 3: Toponium width (full line) and energy splitting for the $V_J$ type potential with different parametrizations, vs. top mass.

radiative corrections give a lower limit, closer to 130 $GeV$, corresponding to a weaker potential. This is shown in the same figure and in fig.3, for a selection of currently proposed potentials.

# 2 DECAY WIDTH AND BRANCHING RATIOS

In what follows, we have approached the problem at the Born level, expecting that if the higher order corrections become too large, an altogether different (presumably non-perturbative) approach should be used. The states we discuss here are $J^{PC} = 0^{-+}$and $1^{--}$, focussing on their leptonic and electromagnetic decay widths. At future large hadron colliders the main production mechanism is through gluon-gluon fusion, as in the case of Higgs production, where, for relatively low mass values, production is dominated [24] by gluonic processes. For $\eta_t$ final state, decay channels include [25] vector boson combinations like $WW$, $ZZ$, $HZ$, $\gamma Z$, $\gamma\gamma$, gluon gluon and all the fermion-antifermion pairs. Of interest here are the decay into two photons[26] or two gluons, for which the following Born level expressions hold ($m$ is the toponium mass):

$$\Gamma_B(\eta_t \to \gamma\gamma) = 12 e_t^4 \alpha^2 \frac{4\pi|\Psi(0)|^2}{m^2} \tag{17}$$

and

$$\Gamma_B(\eta_t \to gg) = \frac{8}{3}\alpha_s^2 \frac{4\pi|\Psi(0)|^2}{m^2} \tag{18}$$

where $|\Psi(0)|$ is the wave function at the origin. Notice, that higher order radiative corrections are expected to reduce these expressions [27] as follows:

$$\Gamma(\eta_t \to \gamma\gamma/gg) = \Gamma_B \left[1 + \frac{\alpha_s}{\pi}\left(\frac{\pi^2}{3} - \frac{20}{3}\right)\right], \tag{19}$$

where $\Gamma_B$ is the Born level decay width . For the vector case, the interesting decay channels are the one in lepton pairs and the one into three gluons, for which one has [26]

$$\Gamma_B(\theta_t \to \mu^+\mu^-) = 4 e_t^2 \alpha^2 \frac{4\pi|\Psi(0)|^2}{m^2} \tag{20}$$

and [28, 29]

$$\Gamma_B(\theta_t \to ggg) = \frac{40(\pi^2 - 9)}{81\pi}\alpha_s^3 \frac{4\pi|\Psi(0)|^2}{m^2} \tag{21}$$

QCD radiative corrections [30] change these expressions into

$$\Gamma(\theta_t \to \mu^+\mu^-) = \Gamma_B(\theta_t \to \mu^+\mu^-)\left[1 - \frac{16}{3}\frac{\alpha_s}{\pi} + O\left(\frac{\alpha_s^2}{\pi^2}\right)\right] \tag{22}$$

and [31]

$$\Gamma(\theta_t \to ggg) = \Gamma_B(\theta_t \to ggg)\left(1 + \frac{\alpha_s}{\pi}\left\{-14.0 + \frac{3}{2}b_0\left[1.161 + \log\left(\frac{2Q}{m}\right)\right]\right\} + O\left(\frac{\alpha_s^2}{\pi^2}\right)\right) \tag{23}$$

respectively. At the Born level, the Coulombic potential (non-relativistic case) gives for the wave-function at the origin

$$|\Psi_{100}(0)|^2 = \frac{1}{\pi}\left(\frac{2}{3}m_Q\alpha_s\right)^3 \tag{24}$$

where $m_Q$ is the mass of the heavy quark. For $\eta_t$ the branching ratios into two photons and into two gluons are then obtained from

$$\Gamma_B(\eta_t \to \gamma\gamma) = \frac{256}{729}\alpha^2\alpha_s^3(Q_s^2)m \tag{25}$$

$$\Gamma_B(\eta_t \to gg) = \frac{32}{81}\alpha_s^2(Q_h^2)\alpha_s^3(Q_s^2)m \tag{26}$$

and from eq.(1) with the toponium width, $\Gamma_{t\bar{t}} = 2\Gamma_t$. In the above equations, we distinguish between a soft and a hard scale, which correspond respectively to the soft gluonic exchanges between the bound quarks and the hard annihilation into two gluons, for which the scale of $\alpha_s$ is of the order of the final state energy. Following the prescription for the argument of $\alpha_s$ given in the previous section, we can write

$$Q_s^2 = \frac{1}{r_B^2} \qquad Q_h^2 = m^2 \tag{27}$$

We now report in Table 1 the values obtained in the Coulomb model, using the one-loop expression for $\alpha_s$ and $\Lambda = 0.2\ GeV$.

**Table 1**

| $m_t$ GeV | $\Gamma_{t\bar{t}}$ GeV | $\alpha_s(Q_s^2)$ $Q_s^2 = m_t E_1$ | $\alpha_s(Q_h^2)$ $Q_h^2 = m^2$ | $\Gamma(\eta_t \to gg)$ MeV | $\Gamma(\eta_t \to \gamma\gamma)$ KeV | $B.R.(\eta_t \to \gamma\gamma)$ – |
|---|---|---|---|---|---|---|
| 100 | 0.187 | 0.196 | 0.119 | 8.4 | 32 | $1.73 \times 10^{-4}$ |
| 110 | 0.390 | 0.192 | 0.117 | 8.4 | 33 | $0.85 \times 10^{-4}$ |
| 120 | 0.650 | 0.189 | 0.116 | 8.6 | 35 | $0.53 \times 10^{-4}$ |
| 130 | 0.970 | 0.187 | 0.115 | 8.7 | 36 | $0.38 \times 10^{-4}$ |

As for vector toponium $^3S_1$, we notice from eq. (20) that, if one neglects spin-spin effects in the potential, the electromagnetic width is simply related to that for the photonic width of the pseudoscalar toponium $^1S_1$ . Thus, at the Born level, and approximating the total width with the electroweak expression, one has

$$BR(\theta_t \to \mu^+\mu^-) = \frac{BR(\eta_t \to \gamma\gamma)}{3e_t^2} \tag{28}$$

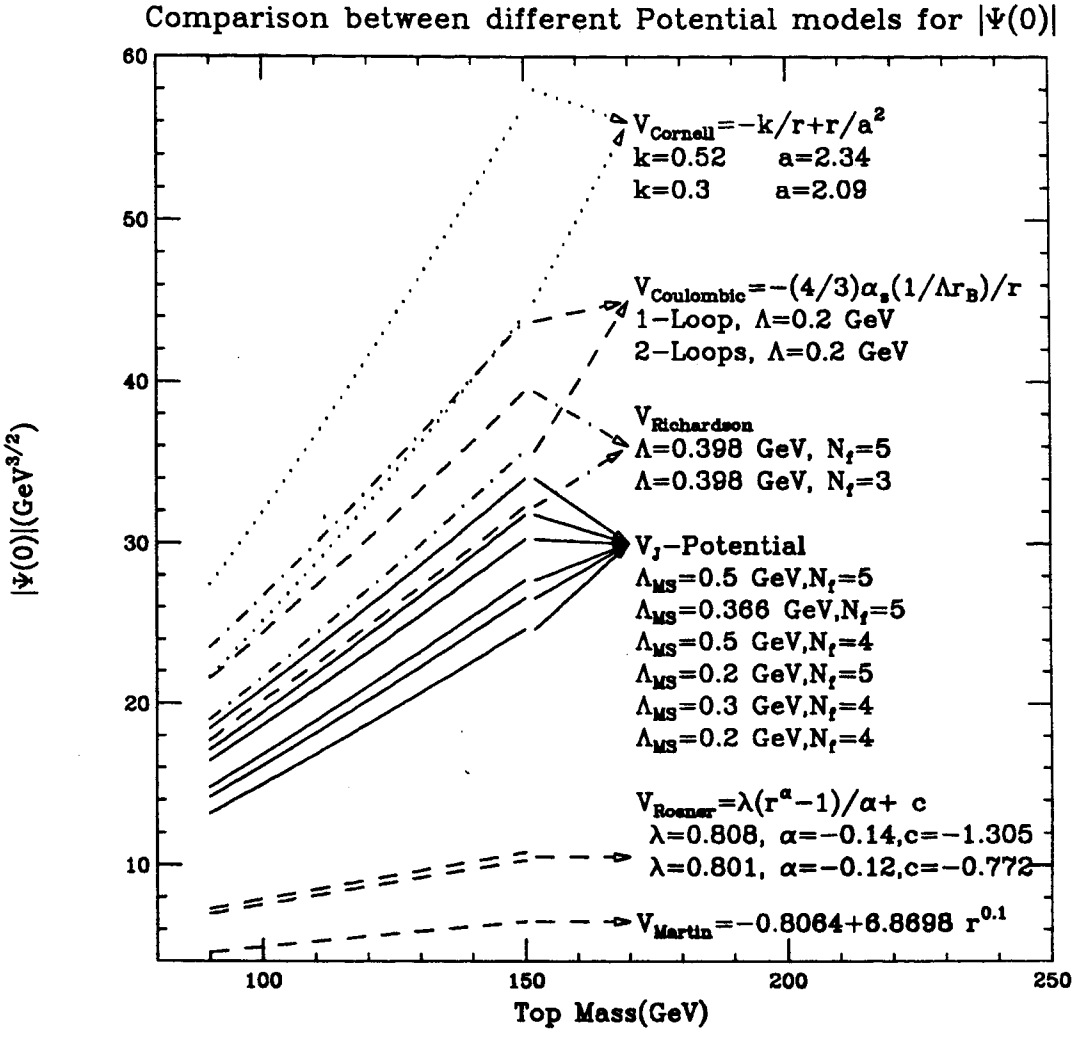


Figure 4: $|\Psi(0)|$ versus top mass for different potential models as indicated in the figure.

and the Branching Ratio for the vector toponium bound state will be quite similar to the one for the pseudoscalar meson.

The estimates shown in Table 1 are very sensitive to the wave function at the origin, which depends upon the choice of potential. As one can see already from Fig.2, the use of the one or two loops expression for $\alpha_s$ in the Coulomb-type potential can give rather different results. Although, in principle, one should already be in a region of $Q^2$ where $\alpha_s$ is small enough for a perturbative calculation, the photonic decay width has an $\alpha_s$ dependence to the cubic power and this can result in rather different predictions for the widths.

A quantitative description of the dependence upon the choice of the potential is shown in Fig.4, where we have calculated $|\Psi(0)|$ for the models described in the previous section.

To better clarify the meaning of certain estimates, we show in Fig.5 the extrapo-

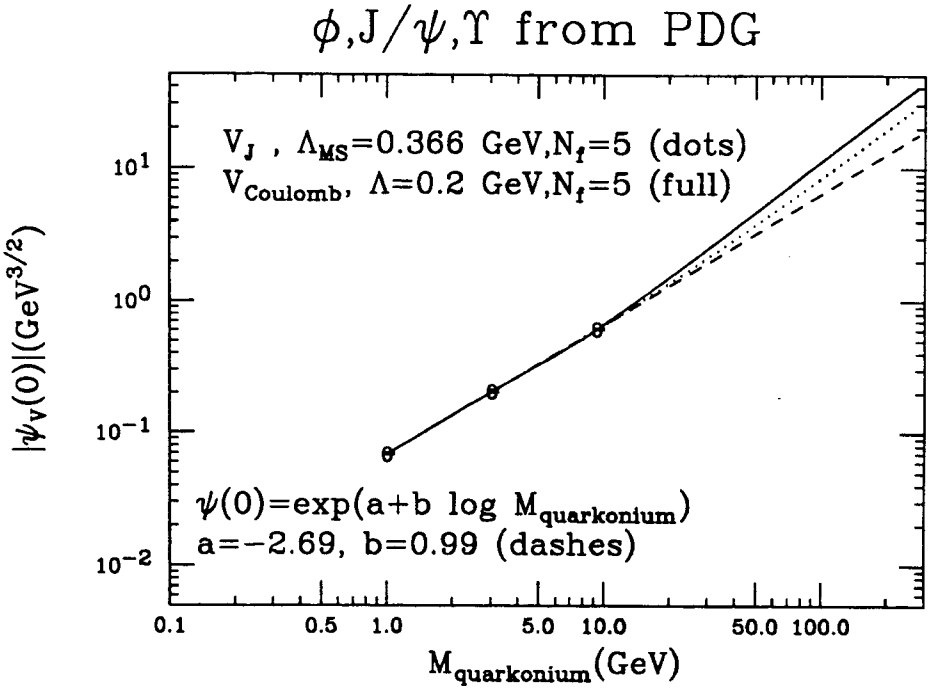


Figure 5: $|\Psi(0)|$ versus quark mass for known vector mesons, and comparison with extrapolations from different potential models as indicated in the figure.

lation from the experimental [32] points for the three vector quarkonia observed so far, the mesons

$$\phi, J/\Psi, \Upsilon \quad .$$

In Fig.5, the wave function at the origin for the three known flavour singlet vector mesons has been calculated from eq. (20), without any radiative corrections, with the experimental data for the electromagnetic widths as input. We notice that a linear extrapolation in the $log-log$ plane, from the three data points to the top mass ranges, reproduces the expectations from the lowest estimate from the $V_J$ potential, while the one–loop Coulombic potential is a $log^2$-type behaviour. The highest estimate from the $V_J-$potentials is in between.

# 3 PRODUCTION CROSS-SECTION

We shall now proceed to calculate the production cross-section at hadron colliders. For a narrow $J = 0$ resonance produced through gluon-gluon fusion, the following expression can be used

$$\sigma(pp \to \eta_t + X) = \frac{\pi^2}{8m^3}\Gamma(\eta_t \to gg)\left(\tau\frac{dL}{d\tau}\right)_{gg} \qquad (29)$$

where, as usual [25],

$$\tau\frac{dL}{d\tau} = \tau\int_\tau^1 \frac{dx}{x} g(x,Q^2)g(\frac{\tau}{x},Q^2)$$

is the gluon-gluon differential luminosity with $\tau = m^2/s$. If there are many narrow bound states, following [33], the wave function at the origin, which enters into the above expression through the width into gluons, can be replaced as follows

$$|\Psi_{100}(0)|^2 \to \sum_n |\Psi_{n,0,0}(0)|^2 \approx |\Psi_{100}(0)|^2\zeta(3) \tag{30}$$

with

$$\zeta(3) = \sum_n \frac{1}{n^3}$$

A calculation and numerical estimate of $\eta_t$ production cross-section was presented in [33], where the expression

$$\sigma_{FKS} = \int_{\tau_0}^{4m_t^2/s} \sigma^{(s)}_{gg\to t\bar{t}} \left(\frac{dL}{d\tau}\right)_{gg} d\tau \tag{31}$$

with

$$\left[\tau_0 \simeq 4(m_b + m_W)^2/s\right]$$

and

$$\sigma^{(s)}_{gg\to t\bar{t}} = \frac{2}{7}\sigma^{(B)}_{gg\to t\bar{t}} \frac{4\pi}{m_t^2\beta_t} ImG^{(s)}_{E+i\Gamma_t}(0,0) \tag{32}$$

was obtained. In the above cross-section , the factor $\frac{2}{7}$ selects the right colour singlet combination from the Born cross-section for $t\bar{t}$ production $\sigma^{(B)}_{gg\to t\bar{t}}$, and $G$ is the Green's function of $t\bar{t}$ system in the colour singlet state. In the narrow width approximation, the cross section of eq.(31) becomes

$$\lim_{\frac{\Gamma}{M}\to 0} \sigma_{FKS} = \frac{\pi^2\alpha_s^2}{6s}\left(\frac{p_s}{m_t}\right)^3 \zeta(3)\left(\frac{dL}{d\tau}\right)_{gg} \tag{33}$$

with

$$p_s = \frac{2}{3}m_t\hat{\alpha}_s \qquad \hat{\alpha}_s = \alpha_s(m_tE_b) \tag{34}$$

which is in fact the exact solution for the Coulomb potential. Indeed, in [33], the argument for $\alpha_s$ is given as

$$Q^2 = m_t\sqrt{E_b^2 + \frac{\Gamma_{t\bar{t}}^2}{4}} \simeq m_tE_b \tag{35}$$

As previously discussed, this value of $Q^2$ is the non–relativistic momentum of a quark of mass $m_t$ in a bound state, when one takes into account reduced mass and finite width effects.

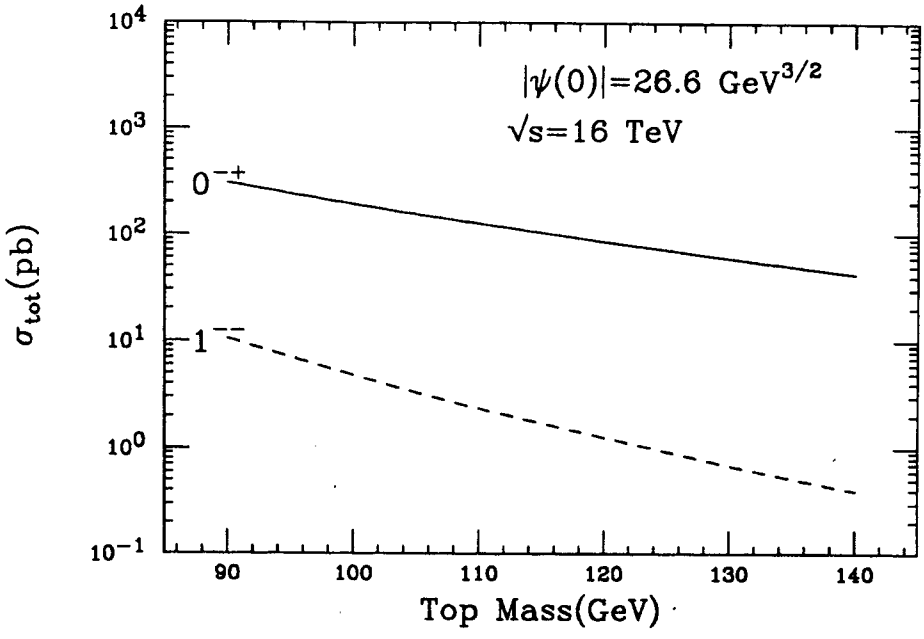


Figure 6: Total production cross-section at LHC for toponium $\eta_t$ (full line) and $\theta_t$ (dashes) for the one-loop Coulomb model, using EHLQ1-type parton densities at LHC.

For the vector toponium state, one can consider both production through the Drell-Yan type process, i.e. $q - \bar{q}$ annihilation, as well as gluon-gluon fusion with inclusive production of a spin one particle $\theta_t$, in association with another gluon. At hadron colliders, in the mass range we are considering, the production cross–section through gluon–gluon fusion is dominant. Using again the narrow–width approximation, one can write

$$\sigma(pp \to \theta_t + X) = \frac{9\pi^2}{8m^3(\pi^2 - 9)}\Gamma(\theta_t \to ggg)\int_{\frac{m^2}{s}}^1 d\tau I(\frac{s\tau}{m^2})\left(\frac{dL}{d\tau}\right)_{gg} \qquad (36)$$

with

$$I(x) = \frac{2}{x^2}\left[\frac{x+1}{x-1} - \frac{2x\ln x}{(x-1)^2}\right] + \frac{2(x-1)}{x(x+1)^2} + \frac{4\ln x}{(x+1)^3}$$

The reduced phase space and one higher power in $\alpha_s$ make the cross-section for vector production smaller by at least one order of magnitude than the one for the pseudoscalar case. Since the branching ratio into the channel of interest is of the same order of magnitude as for the case of $\eta_t$, it is clear that the vector case is much more difficult to study at hadron colliders than the pseudoscalar one. The dominant gluon-gluon production cross-sections for the pseudoscalar and vector toponium states at LHC, using EHLQ1 [34]-type densities are shown in Fig.6, for the one-loop Coulomb potential. As it is clear from the previous section, these estimates can be considered as "the most

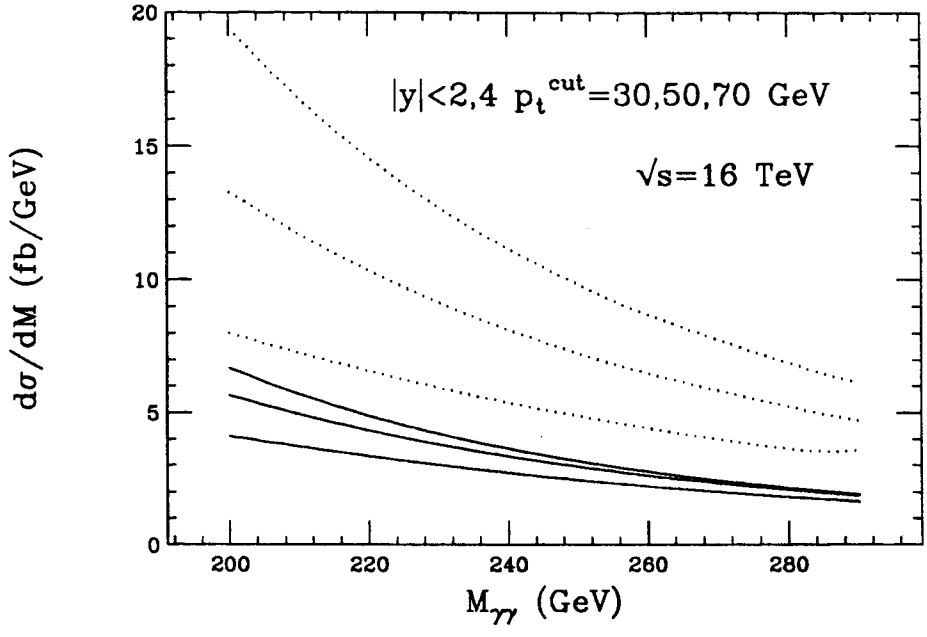


Figure 7: Differential cross-section for $q - \bar{q}$ annihilation to two photons at LHC, with rapidity cut on each photon $|y| \leq 2$(full) and 4 (dots), and different transverse momentum cuts, $p_t^7 \geq 30, 50$ and 70 $GeV$.Densities are HMRSB type.

optimistic" ones, but we can learn from them that search for the vector state will be exceedingly difficult, since vector production is more than one order of magnitude lower than the pseudoscalar one, as discused above.

These cross-sections indicate the possibility of detection only for the pseudoscalar state, and only if the top quark has a mass around 100-120 $GeV$. In fact the total production cross-section, $\approx$ 100 $pb$ , with a $10^{-4}$ branching ratio into two photons, leads to about 1000 events for an integrated LHC luminosity of $10^2 fb^{-1}$. Even then, the observability of a possible signal crucially depends on the physics background, to which we now turn in the next section.

# 4 BACKGROUND EVALUATION

The irreducible QCD background to the two photon decay channel comes from three possible processes, the Born term, i.e. $q\bar{q} \rightarrow \gamma\gamma$, the bremsstrahlung contributions [35] $qg \rightarrow q\gamma\gamma$, and the box diagrams [36, 37] $gluon\ gluon \rightarrow \gamma\gamma$.

In the above processes, the Born and the bremsstrahlung terms have singularities for small transverse momentum of the emitted photons, which make them quite larger (by as much as one order of magnitude) than the signal. To reduce the background, one must impose kinematic cuts both in rapidity as well as on the photon transverse

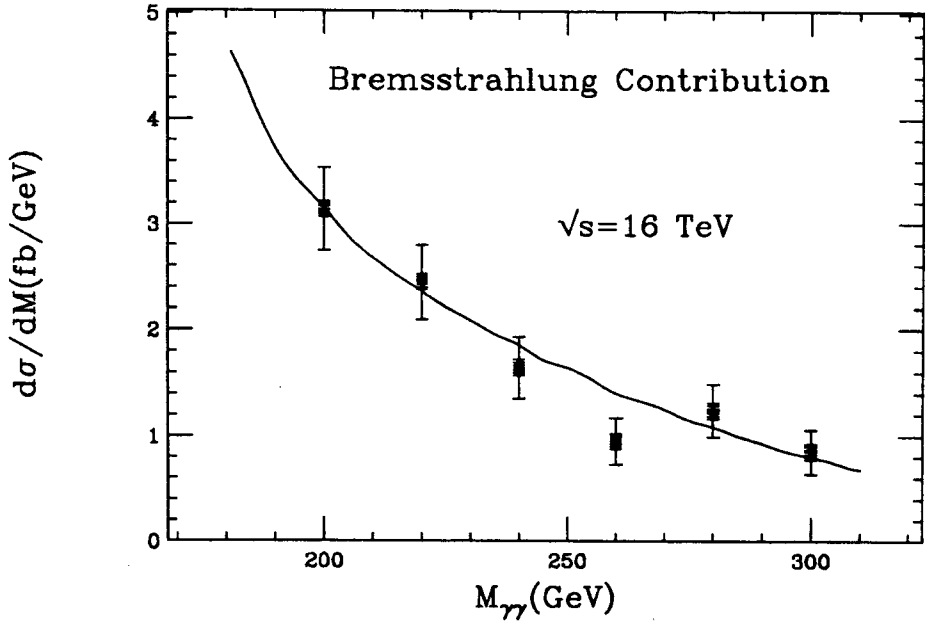


Figure 8: Differential cross-section for two photon production from initial quark-gluon processes, at LHC, with rapidity cut on each photon $|y| \leq 2$ and transverse momentum cut $p_t^\gamma \geq 70\ GeV$ and isolation cut . Data points are Montecarlo calculation from ref.[38], full line is extrapolation. Densities are from [39].

momentum. In Fig.7 we show the differential cross-section for the annihilation process, and for different cuts on the photon transverse momentum. The effects of rapidity cuts, $y \leq 2,4$ are also shown. The bremsstrahlung diagrams which contribute to the background are quite a few. An evaluation by C.Seez [38], in which both a transverse momentum cut as well as an isolation cut are imposed, gives the results shown in Fig.8.

The kinematic cuts have the effect of reducing the bremsstrahlung as well as the Born term contribution to a few femtobarn per GeV. This cross-section is now comparable to the one obtainable from the signal. We have in fact seen in the previous section, that in the top mass range around 100 $GeV$, the signal can be estimated to give a cross-section $\approx 10 - 20 fb$.

The other important background contribution comes from gluon-gluon fusion into two photons. In the mass range of interest, this process, at LHC/SSC, will give a contribution of the same order of magnitude as the previous ones. The large gluon densities in fact compensate for the extra powers in $\alpha_s$ and make mandatory the inclusion of these contributions. For this process, the dependence of the amplitudes from the internal quark masses has been discussed in [37].

In Fig. 9, we have fixed the top mass to be 100 GeV, so as to evidentiate how this contribution depends upon the kinematic cuts. Then, for a specific set of cuts,

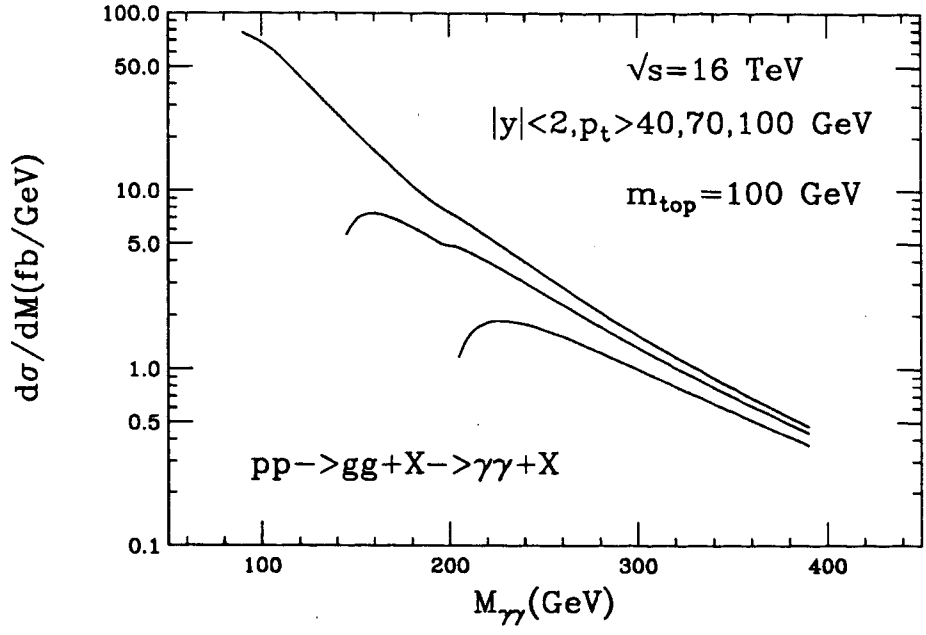


Figure 9: Differential cross-section for two photon production from gluon gluon fusion, at LHC,with internal heavy quark mass and cuts as indicated, and densities from [39].

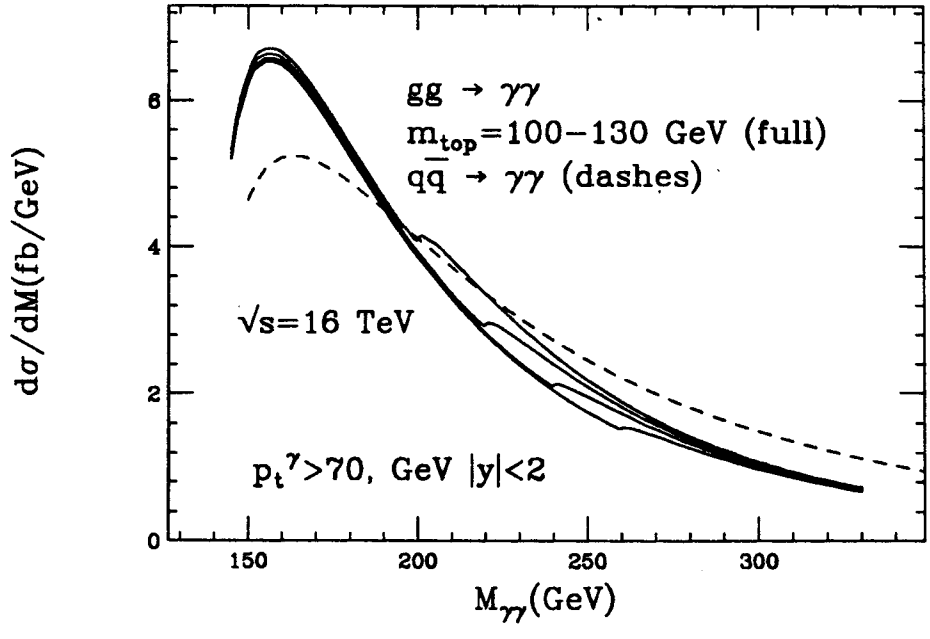


Figure 10: Differential cross-section for two photon production from initial gluon-gluon processes, at LHC, for different values of the internal heavy quark mass, as indicated (full lines), and from the $q\bar{q}$ contribution (dashed line). Densities are from [39].

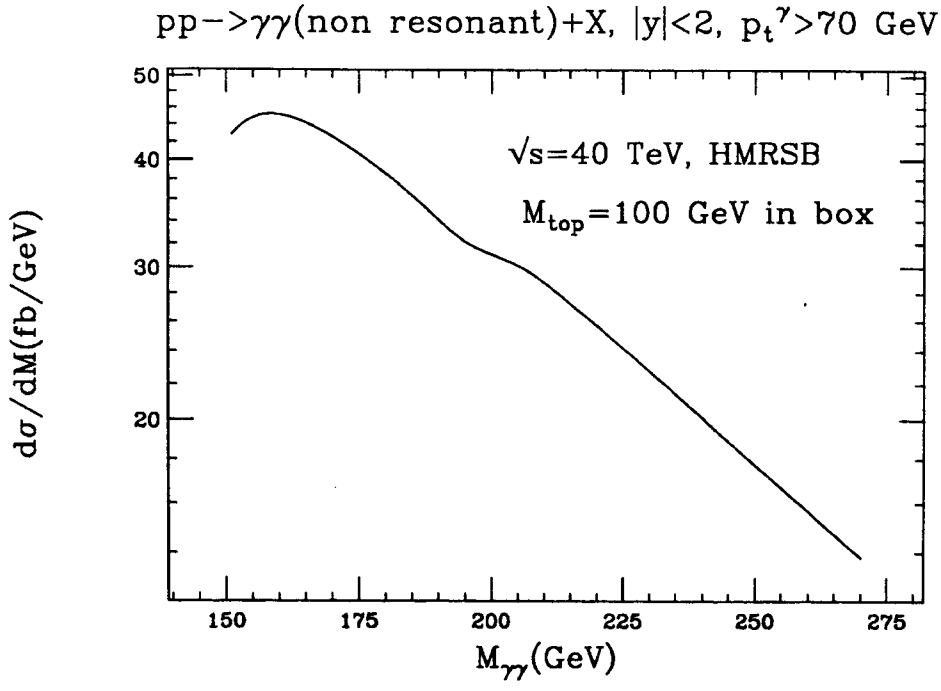


Figure 11: Differential cross-section for two photon production (other than toponium ) at SSC, with densities from HMRSB [39].

we have let the internal heavy quark mass vary. This is illustrated in Fig. 10. For the SSC case, one can evaluate the background in a similar fashion. We have calculated the Born process and the gluon-gluon fusion with the same cuts as for LHC. As for the bremsstrahlung, we have taken its contribution after cuts to be the same as the one from gluon-gluon fusion. The total background contribution one can expect from the above irreducible processes at SSC, is shown in Fig. 11.

# 5 SIGNAL CROSS-SECTION FOR $pp \to \gamma\gamma + X$

In order to estimate the signal cross section for the process

$$pp \to \eta_t + X \to \gamma\gamma + X$$

one needs to take into account the experimental resolution for the proposed LHC or SSC detectors. In general, one has

$$\frac{d\sigma}{dM} = \frac{(\sigma_\eta \cdot BR)}{\sqrt{2\pi}\sigma_G} \cdot \exp\left[-(M - m_{t\bar{t}})^2/2\sigma_G^2\right], \tag{37}$$

where $\sigma_\eta \cdot BR$ is the total production cross-section in the given final state with branching ratio BR. The gaussian width $\sigma_G$ is the sum in quadrature of the natural width

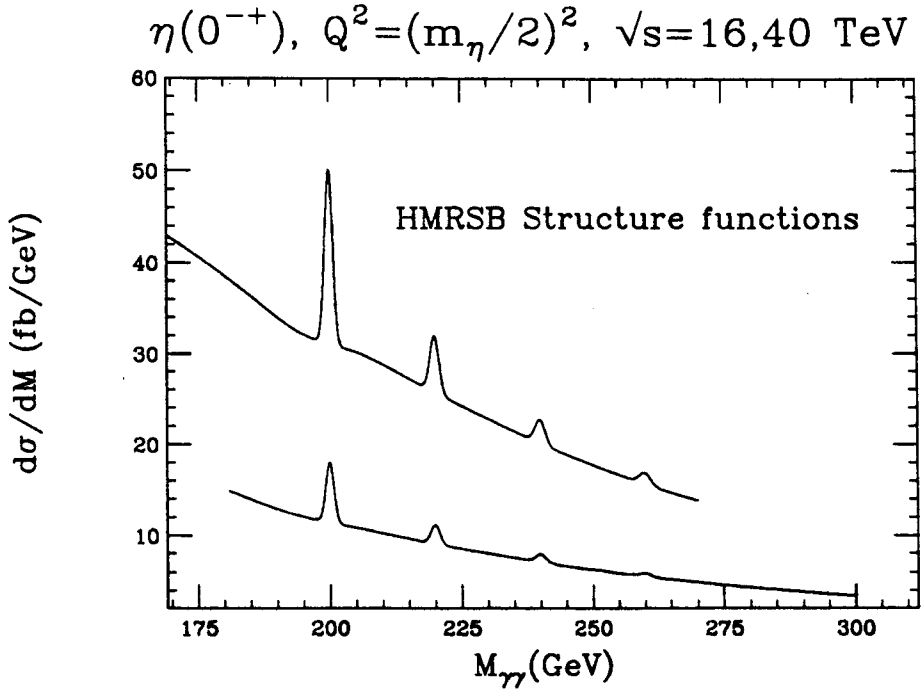


Figure 12: Differential cross-section for two photon production at LHC and SSC, with rapidity cut on each photon $|y| \leq 2$ and transverse momentum cut $p_t^\gamma \geq 70\ GeV$. Densities are from HMRSB [39].

and the experimental resolution, i.e. $\sigma_G = \sqrt{\sigma_{nat}^2 + \sigma_{exp}^2}$ where $\sigma_{nat} = \frac{\Gamma_{t\bar{t}}}{2.35}$ and $\sigma_{exp}$ is the experimental resolution, which depends upon the calorimeter used in the detection. We assume the particular conditions described in [24, 38], with an experimental resolution given by

$$\frac{\Delta E}{E} = \frac{0.02}{\sqrt{E}} \quad \textit{with a constant term } \frac{1}{2}\% \tag{38}$$

and show in Fig. 12 the results we obtain for different values of the top mass. The signal cross section of this figure includes both background and signal, for the one loop Coulomb model, for SSC and LHC, respectively. We notice that the clear peak at $m_{top} = 100\ GeV$ is now excluded by the recent CDF [4] limits and possible searches for this state can only concentrate on the higher mass values. Notice also, as discussed previously, that a two-loop Coulomb model will give cross-sections and branching ratios such that the peak values will be reduced by at least a factor 4. For such potentials, the observability of the signal, even for the higher mass values, may then disappear. The signal cross-section shown in the figure has been computed with the experimental resolution of eq.(38), with

$$\sigma_G = \Delta m_{\gamma\gamma} \approx \sqrt{2}\Delta E \textit{ and } \Gamma_{t\bar{t}} = 2\Gamma_t$$

which correspond to natural and gaussian widths shown in table 2.

Table 2

| *Top mass* *GeV* | $\sigma_{nat}$ *GeV* | $\sigma_{exp}$ *GeV* | $\sigma_G$ *GeV* | $\Gamma_{t\bar{t}}$ *GeV* |
|---|---|---|---|---|
| 100 | 0.0795 | 0.762 | 0.766 | 0.187 |
| 110 | 0.167 | 0.833 | 0.849 | 0.390 |
| 120 | 0.278 | 0.903 | 0.945 | 0.650 |
| 130 | 0.413 | 0.974 | 1.060 | 0.970 |
| 140 | 0.568 | 1.045 | 1.189 | 1.334 |
| 150 | 0.750 | 1.116 | 1.345 | 1.763 |

We see from the above table that the experimental resolution dominates the signal width for low values of the top quark mass. For a heavier top, $\approx$ 120 $GeV/c^2$ and above, the two become comparable and the signal becomes more and more diffuse.

Before computing the statistical significance of the signal cross-sections, let us briefly discuss the QCD potential model predictions. For the $V_J$ potential, for the most optimistic of the two cases discussed in [6], we show in Fig. 13 the inclusive production cross-section with and without cuts, at LHC, and using both EHLQ1 [34] type densities as well as HMRSB [39]. Relative to the estimates of Sect.3, these cross-section are a

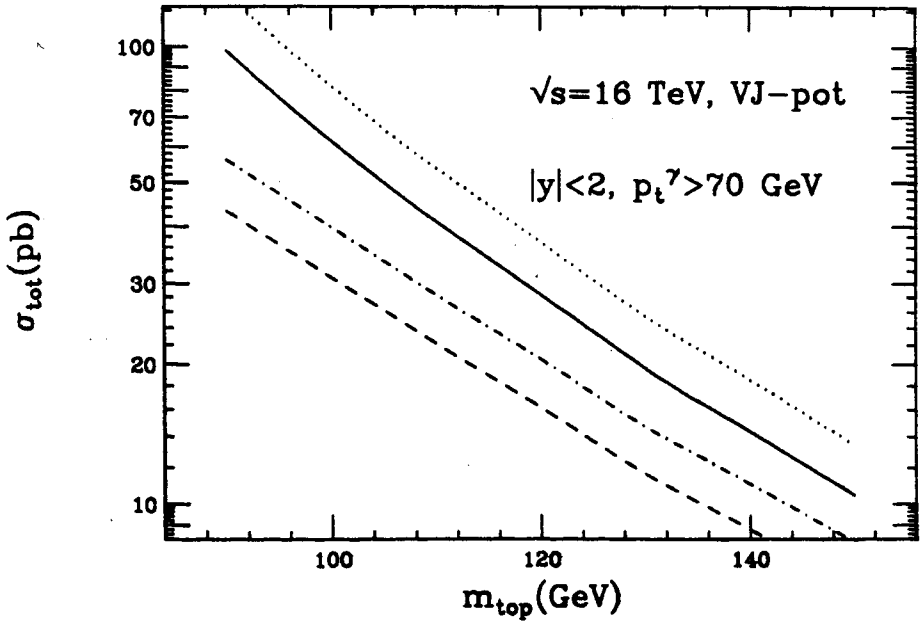


Figure 13: Total Production cross-section for toponium with QCD-type potential models, with and without cuts for EHLQ1 densities(dots/dotdash) and HMRSB(full/dashes).

factor 2 lower. When folded with the branching ratios, the signal cross-sections will be 4-5 times smaller, as already noticed [6].

# 6 STATISTICAL SIGNIFICANCE

One can evaluate the statistical significance for this signal at LHC, by plotting the

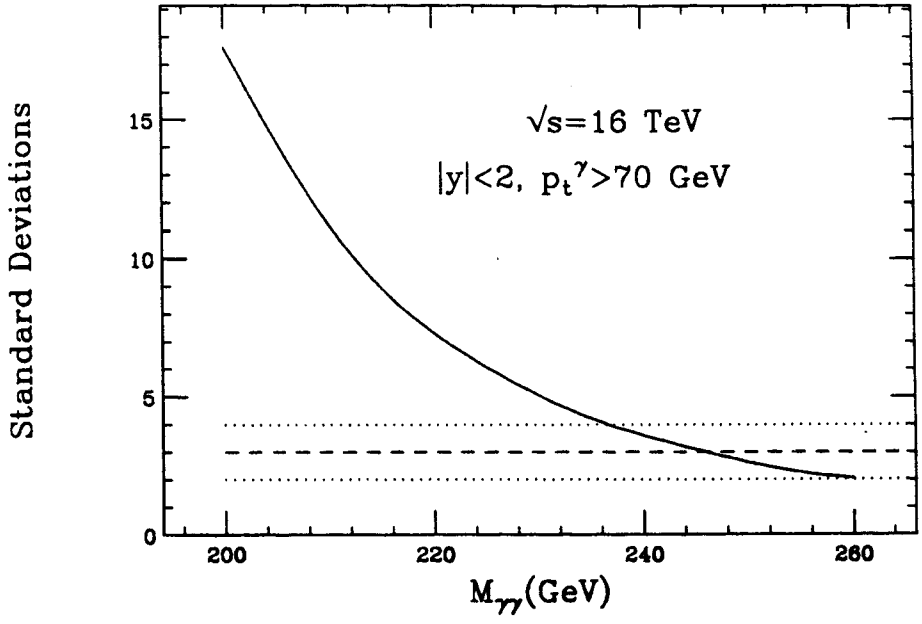


Figure 14: Number of standard deviations for toponium detection into two photon final state at LHC.

signal level above noise $S = N_{signal}/\sqrt{N_{signal} + N_{bck}}$. For the signal, the number of events is estimated by taking all the events around the resonance peak, within a mass bin $\Delta M = \Gamma_{t\bar{t}}$. This amounts to 85 % of the peak cross-section. The number of background events contained in the same mass bin is then obtained from

$$N_{bck} \simeq \frac{d\sigma}{dM}|_{m_{t\bar{t}}} \cdot 3\sigma_G \tag{39}$$

where $\sigma_G$ is the gaussian width.

We show in Fig. 14 the statistical significance of this signal at LHC, using the one–loop Coulomb potential discussed previously. These estimates are based on a luminosity of $10^{34} cm^{-2} sec^{-1}$ and $\Delta t = 10^7$ *sec.*. As pointed out in [6], for the case of the $V_J$–potential the signal is reduced by at least a factor 4, and thus it will remain below the noise level for any acceptable value of the top mass. In the SSC case, the situation, at least for the low luminosity option $L = 10^{33}\ cm^{-2}\ sec^{-1}$, is even worse: the background and signal increase by a factor $\approx 2 - 3$, but the luminosity would be smaller by a factor 10 and the observability limit would be reached earlier. Only the high luminosity SSC option, [7], i.e. $L = 10^{34}\ cm^{-2}\ sec^{-1}$ could still leave some

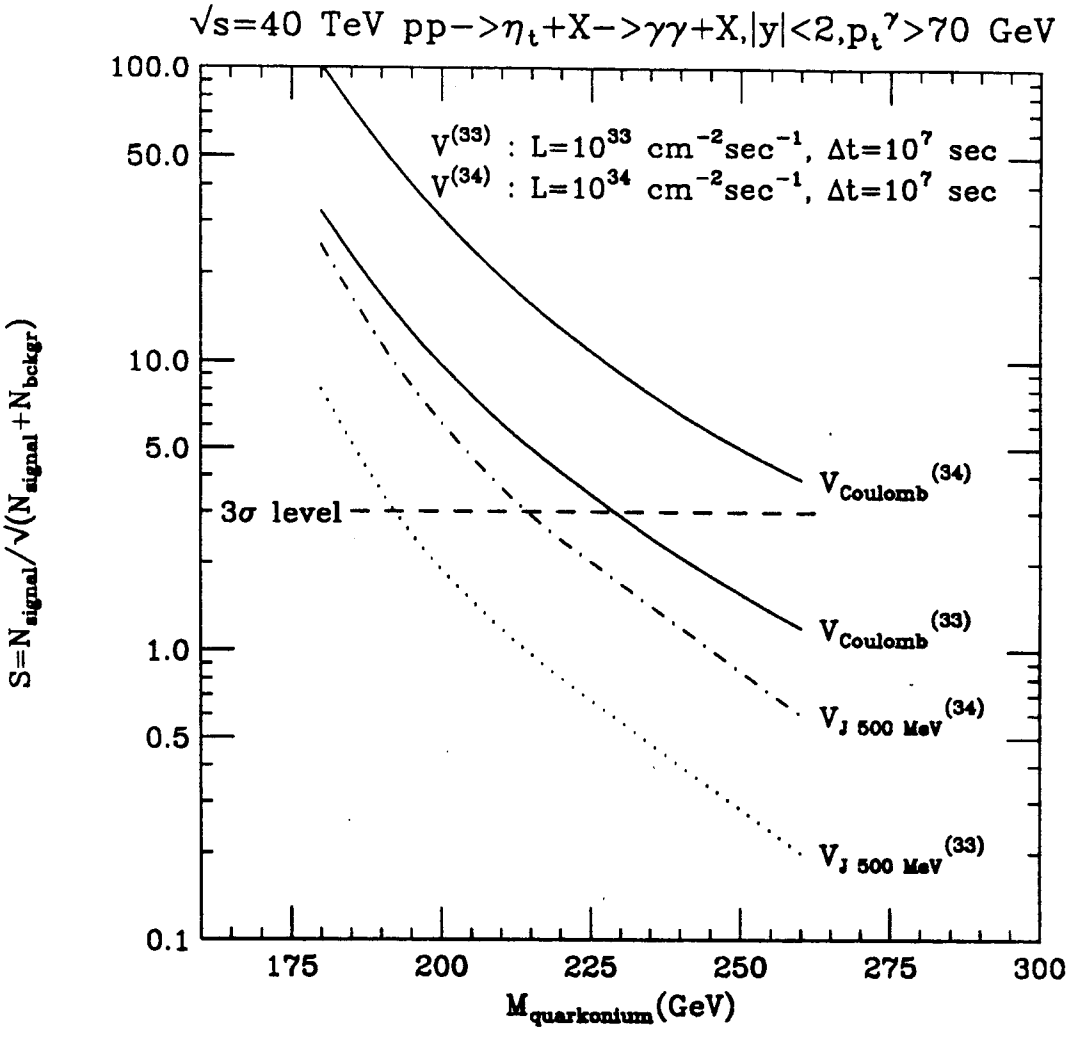


Figure 15: Number of Standard Deviations at SSC with one-loop Coulomb and $V_J$ potential, for different SSC luminosities.

window of detectability. It should be noticed that, even in this case, it is not clear as to whether it would be possible to obtain the extreme conditions described previously for the experimental apparatus.

For a possible high experimental resolution case, we nonetheless show, in Fig. 15, the signal to noise ratio at SSC, with two different luminosity options, using for the signal cross section two different potential models, the one-loop Coulomb model and the most optimistic case for the $V_J$ potential.

# 7 CONCLUSIONS

The possibility of observing toponium bound states at LHC and SSC has been discussed for different luminosity options, and for a very precise detector configuration. The sensitivity of the signal cross-section from the interquark potential has been high-

lighted. It appears that present limits on the top mass, almost but all exclude the possibility of formation and subsequent detection of the bound states.

# References


[1] CDF Collaboration, F. Abe et al., *Phys Rev. Lett.* **64** (1990) 142, 147; ibidem **68** (1992) 447.

[2] I.Bigi, Y.Dokshitzer, V.Khoze, J.Kuhn and P. Zerwas, *Phys. Lett.* **B181** (1986) 157.

[3] M.Narain (D0 Collaboration), *Search for the top quark* , presented at the 28th Rencontres de Moriond, Les Arcs 20-26 March 1993.

[4] A.Caner (CDF Collaboration), *Top Search at CDF* presented at the 28th Rencontres de Moriond, Les Arcs 20-26 March 1993.

[5] G.Pancheri, J.-P. Revol and C.Rubbia, *Physics Letters* **B277** (1992) 518.

[6] J. H. Kuhn and E. Mirkes, *Physics Letters* **B296** (1992), 425.

[7] R. Schwitters, *Future Hadron Colliders: the SSC*, XXVI International Conference on High Energy Physics, August 6-12 1992, Dallas, Texas.

[8] V. Barger, H. Baer, K.Hagiwara and R. J. N. Phillips, *Phys. Rev.* **D30** (1984) 947.

[9] V. S. Fadin, V. A. Khoze, *JEPT Lett.* **46** (1987) 525; *Yad. Fiz.* **48** (1988) 487.

[10] A.Billoire, *Phys. Lett.* **B92** (1980) 343.

[11] H. Inazawa and T.Morii, *Phys. Lett.* **203B** (1988) 279.

[12] M.J.Strassler and M.E.Peskin, *Phys.Rev.* **D43** (1991) 1500.

[13] W.A.Bardeen, A.J.Buras, D.W.Duke and T.Muta, *Phys. ReV.* **D18** (1978) 3998; W.J. Marciano, *Phys. Rev.* **D29** (1984) 580.

[14] E. Eichten, K. Gottfried, T. Kinoshita, K. D. Lane, T. M. Yan, *Phys. Rev.* **21D** (1980) 203.

[15] J.L. Richardson, *Phys. Lett.* **82B** (1979) 272.

[16] J.H.Kuhn and S.Ono, *Zeit Phys.* **C21** (1984) 385; K.Igi and S.Ono, *Phys. Rev.* **D33** (1986) 3349.

[17] W.Buchmuller and S.-H.H.Tye, *Phys. Rev.* **D24** (1981) 132.

[18] J. H. Kuhn and P. Zerwas, *Phys. Rep.* **167** (1988) 321, and references therein.

[19] A. Martin, *Phys. Lett.* **93B** (1980) 338 and *Phys. Lett.* **100B** (1981) 511.

[20] M. Mahchacek, Y. Tomozawa, *Ann. Phys. (NY)* **110** (1978) 407.

[21] C. Quigg, J. Rosner, *Comments Nuclear Particle Physics* **8** (1978) 11.

[22] A. K. Grant, J. L. Rosner, E. Rynes; *Phys. Rev.* **D47** (1993) 1981.

[23] We thank C. Natoli for providing the numerical program, as from C.R.Natoli et al., *Phys. Rev.* **A 22** (1980) 1104.

[24] Z. Kunst, W. J. Stirling, Large Hadron Collider workshop, Aachen, 4-9 October 1990.

[25] V.D.Barger and R.J.N.Phillips,*Collider Physics*, Addison- Wesley 1988.

[26] R.Van Royen and V.Weisskopf, *Nuovo Cimento* **50A** (1967) 617.

[27] R.Barbieri, G.Curci, E. d'Emilio and R. Remiddi, *Nuclear Phys.* **B154** (1979) 535.

[28] T. Appelquist and H. Politzer, *Phys. Rev. Lett.* **34** (1975) 43.

[29] A.De Rujula and S.L.Glashow, *Phys. Rev. Lett.* **34** (1975) 46.

[30] R.Barbieri, R. Gatto, R. Kogerler and Z.Kunszt, *Phys. Lett.* **57B** (1975) 455;W. Celmaster, *Phys. Rev.* **D19** (1979) 1517.

[31] P. B. MacKenzie and G. Lepage, *Phys. Rev. Lett.* **47** (1981) 1244.

[32] Particle Data Group, *Phys. Rev.* **D45** (1992) 1.

[33] V.Fadin, V.Khoze and T.Sjostrand, *Zeit Physics* **C48** (1990) 613.

[34] E. Eichten, I. Hinchliffe, K. Lane and C. Quigg, *Rev. of Mod. Physics* **56** (1984) 579; **57** (1986) 1065 (E).

[35] P.Aurenche, A.Douiri, R.Baier, M.Fontannaz and D.Shiff, *Z.Phys.* **C29** (1985) 459.

[36] Ll. Ametller, A.Gava, N.Paver and D. Treleani, *Phys. Rev.* **D32** (1985) 1699.

[37] A.W.N.Glover and M.J.J. Van der Bij, *Phys. Lett.* **B206** (1988) 701.

[38] C. Seez et al., *"Photon decay modes of the intermediate mass Higg"*, Proc. Large Hadron Collider Workshop, Aachen, 4-9 October 1990 and private communication.

[39] P.N.Harriman, A.D.Martin, W.G.Sterling and R.G. Roberts, *Phys.Rev.* **D42** (1990) 798.